J|A|C|S COMMUNICATIONS

Published on Web 12/15/2010

Highly Aminated Mesoporous Silica Nanoparticles with Cubic Pore Structure

Teeraporn Suteewong,[†] Hiroaki Sai,[†] Roy Cohen,[‡] Suntao Wang,[§] Michelle Bradbury,[||] Barbara Baird,[‡] Sol M. Gruner,[§,⊥] and Ulrich Wiesner*[,†]

Departments of Materials Science and Engineering, Chemistry and Chemical Biology, and Physics, Cornell University, Ithaca, New York 14853, United States, Department of Radiology, Memorial Sloan-Kettering Cancer Center, 1275 York Avenue, New York, New York 10065, United States, and Cornell High Energy Synchrotron Source (CHESS), Cornell University, Ithaca, New York 14853, United States

Received July 12, 2010; E-mail: ubw1@cornell.edu

Abstract: Mesoporous silica with cubic symmetry has attracted interest from researchers for some time. Here, we present the room temperature synthesis of mesoporous silica nanoparticles possessing cubic $Pm\bar{3}n$ symmetry with very high molar ratios (>50%) of 3-aminopropyl triethoxysilane. The synthesis is robust allowing, for example, co-condensation of organic dyes without loss of structure. By means of pore expander molecules, the pore size can be enlarged from 2.7 to 5 nm, while particle size decreases. Adding pore expander and co-condensing fluorescent dyes in the same synthesis reduces average particle size further down to 100 nm. After PEGylation, such fluorescent aminated mesoporous silica nanoparticles are spontaneously taken up by cells as demonstrated by fluorescence microscopy.

Significant research efforts in recent years have been devoted to the development of nanoparticles for applications in biomedical imaging, sensing, and drug delivery.[1−4] Nanoparticle architecture and composition are key to the achievable property profiles. Silica is one of the most studied nanoparticle matrix materials due to low toxicity, versatile bulk and surface chemistry, and biocompatibility.[5−9] Ordered mesoporous silica in particular has attracted considerable interest due to its ability to reversibly load other compounds. It provides high surface area and large pore volume, necessary in sorption and catalysis applications, while maintaining the intrinsic properties of silica.[10,11] Mesoporous siliceous materials with three-dimensional pore systems, such as MCM-48, provide advantages in diffusion and transport over one-dimensional channel systems such as in MCM-41-type materials.[6,11,12]

Among several three-dimensional mesoporous structures reported, mesoporous silica with cubic $Pm\bar{3}n$ symmetry and possessing a cage-type structure that is three-dimensionally interconnected with small open windows is a promising material, for example, as a carrier for biologically active molecules.[12,13] Compared to cubic MCM-48 materials, only a few studies report on $Pm\bar{3}n$-type silica.[14−18] Recently, amine functionalized $Pm\bar{3}n$ mesoporous silica prepared from co-condensation of 3-aminopropyl triethoxysilane (APTES) and tetraethyl orthosilicate (TEOS) was reported.[19] Although with 4%, the mole percentage of APTES relative to total silane precursors (TEOS and APTES) was low, this work broadened the composition and functionality range of cage-type mesoporous silica. Cubic $Pm\bar{3}n$ mesoporous silica nanoparticles from high (>50 mol %) amino silane feed have not yet been reported. Furthermore, the existing synthesis protocol of amine containing $Pm\bar{3}n$ mesoporous silica only yielded micrometer-sized particles.[19] This may affect their applicability to bio-related applications, particularly, cellular uptake, which is known to be strongly size dependent.[20−22]

Herein, we report the room temperature synthesis of discrete, faceted $Pm\bar{3}n$ highly aminated mesoporous silica nanoparticles (NH_2-MSNs), from 54 mol % APTES. To our surprise, the synthesis protocol is quite robust allowing the co-condensation of other functional moieties in the same synthesis, for example, organic dyes, without appreciable loss of structure control. We further demonstrate that the addition of pore expander 1,3,5-trimethylbenzene (TMB) to the synthesis increases pore size from 2.7 to 5 nm while decreasing overall particle size. Rendering these highly aminated, pore-expanded particles fluorescent by co-condensing organic dyes into the particles reduces particle size even further, down to about 100 nm, the smallest average particle size observed in this study. Finally, using fluorescence microscopy, we show the first results cellular uptake of such highly aminated MSNs after surface PEGylation.

In general, NH_2-MSNs were prepared via base-catalyzed sol−gel silica reactions using hexadecyltrimethyl ammonium bromide (CTAB), TEOS, and high molar amounts of APTES in the presence of ethyl acetate (see Supporting Information).[23] Reactions proceeded for 24 h at room temperature. CTAB was removed by either acetic acid extraction or calcination. TEM images of acid-treated materials (Figure 1a−c) reveal discrete and well-faceted mesoporous particles. The size of the smallest particles in Figure 1a is down to about 100 nm, while the size of the largest particles is above 200 nm. For the larger particles, a truncated-octahedral shape can clearly be discerned from these images. Average particle size, as obtained from TEM image analysis, is about 220 ± 50 nm, which is consistent with the hydrodynamic particle size of 220 nm determined from dynamic light scattering (DLS) (see Supporting Information). Two projections of a truncated, octahedrally shaped particle exhibiting four-fold and three-fold symmetries, that is, along the [100] and [111] directions are shown in Figure 1, panels b and c, respectively. Both these projections, as well as the particle shape, suggest a cubic structure for these materials.

To further characterize the structure of the particles, small-angle X-ray scattering (SAXS) was employed. SAXS patterns of dried powders of acid extracted and calcined materials are presented in Figure 2, panels a and b, respectively. On first inspection, the SAXS pattern of the calcined sample is shifted to higher q-values, where q denotes the scattering vector and is defined as $q = 4\pi \sin \theta/\lambda$ with a scattering angle of 2θ and the X-ray wavelength $\lambda = 1.54$ Å. This shift likely results from a contraction of the siliceous matrix induced by further silica condensation upon calcination. Twelve peaks consistent with the (110), (200), (210), (211), (220), (310),

[†] Department of Materials Science and Engineering, Cornell University.
[‡] Department of Chemistry and Chemical Biology, Cornell University.
[§] Department of Physics, Cornell University.
[||] Memorial Sloan-Kettering Cancer Center.
[⊥] Cornell High Energy Synchrotron Source (CHESS).

10.1021/ja1061664

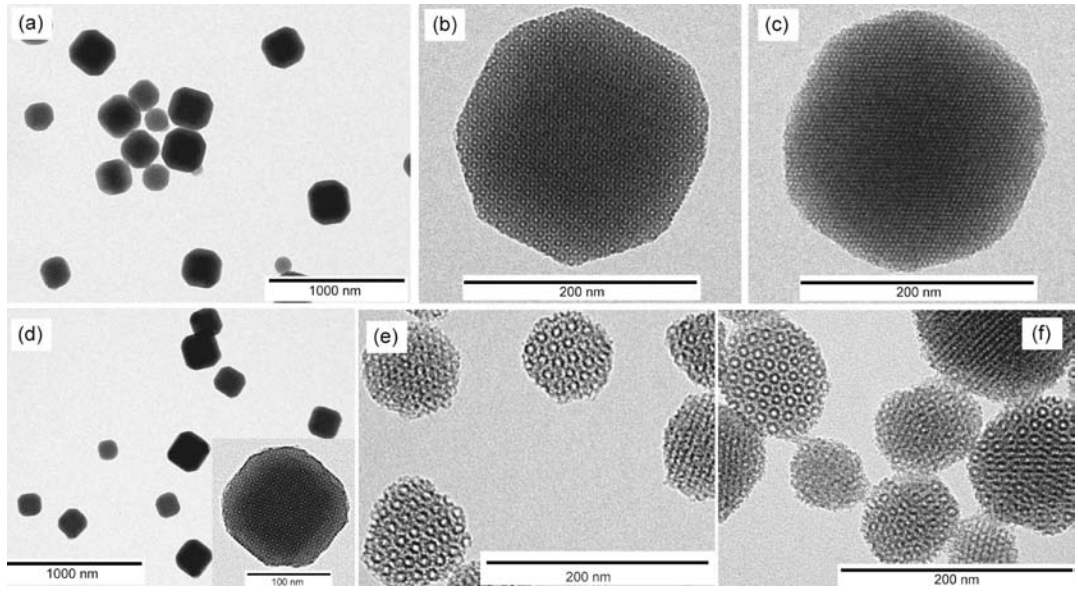

Figure 1. TEM images of (a) NH_2-MSNs at low magnification, (b) NH_2-MSN at [100] projection, (c) NH_2-MSN at [111] projection, (d) TRITC-labeled NH_2-MSNs (inset: high magnification image at [100] projection), (e) large-pore NH_2-MSNs, and (f) TRITC-labeled large-pore NH_2-MSNs.

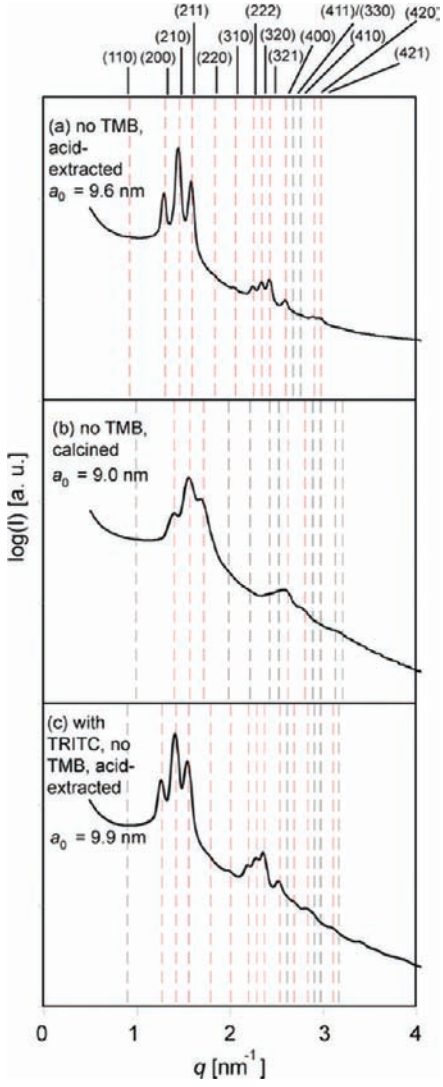

Figure 2. SAXS patterns of (a) acid-extracted and (b) calcined NH_2-MSNs and (c) acid-extracted TRITC-labeled NH_2-MSNs.

(222), (320), (321), (400), (420), and (421) indices of a cubic lattice can be observed in the pattern of the acid-extracted material (Figure 2a; see Supporting Information for details). Allowed peaks corresponding to $Pm\bar{3}n$ symmetry are indicated in Figure 2 by vertical lines. Red lines are the observed peaks, while black lines indicate allowed positions missing in the scattering patterns. Albeit not as well resolved, at least five of the expected peaks for a $Pm\bar{3}n$ lattice can be observed for the calcined material (Figure 2b). The pattern in Figure 2a was taken at the Cornell High Energy Synchrotron Source (CHESS), while the pattern of the calcined sample was taken at a rotating anode setup. We speculate that the peaks in Figure 2b are more poorly resolved than in Figure 2a, both because of the intrinsically poorer resolution of the laboratory setup and because the specimen is intrinsically more disordered. The SAXS and TEM results combined are consistent with a cubic $Pm\bar{3}n$ symmetry for the acid extracted sample, with unit cell dimension (a_0) = 9.6 nm. If one assumes that the calcined material has the same symmetry and the strongest peak is the (210) peak, then the unit cell dimension is 9.0 nm.

The use of organosilane at high molar ratio in the co-condensation based sol−gel synthesis usually affects the packing of surfactant−silane complexes and hence causes the formation of disordered mesostructures.[19,24] In contrast, in the present study, the amino groups are incorporated in the silica matrix without sacrificing pore size and morphology control.[25] High amine content in these particles is reflected by a strongly positive zeta potential of the acid-extracted particles in water, that is, 42 ± 5 mV (see Supporting Information). In comparison, the reported zeta potential for non-aminated MCM-41-type MSNs is approximately −35 mV, that is, highly negative as expected from the low isoelectric point (pH 2−3) of pure silica.[26] N_2 sorption isotherms of acid-extracted and calcined mesoporous nanoparticles exhibit a type IV isotherm with small and narrow hysteresis loops at high relative pressure, which are due to incomplete desorption of N_2 from micropores (Figure 3a).[10] The BET surface area of the calcined sample is 1264 $m^2\ g^{-1}$, and is almost 2 times higher than that of the acid-extracted sample, 674 $m^2\ g^{-1}$. Thermogravimetric analysis (see Supporting Information) suggests this to be the result of the degradation of the high amounts of organic moieties of APTES. In contrast, the pore sizes calculated using the BJH method of acid-extracted and

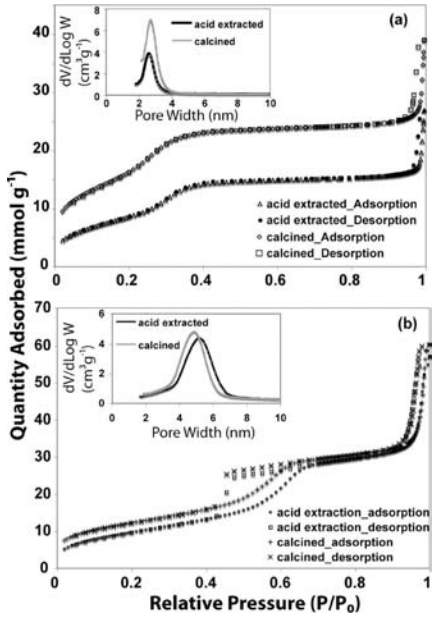

Figure 3. N_2 sorption isotherms (inset: BJH pore size distribution from adsorption branches) of (a) template-removed NH_2-MSNs and (b) template-removed large-pore NH_2-MSNs. For each particle case, two data sets are shown corresponding to acid-extracted and calcined samples, respectively.

calcined NH_2-MSNs (Figure 3a, inset) are the same, that is, 2.7 nm. The BJH model assumes cylindrical pores and thus underestimates the true pore size. We thus also estimated the pore size as 3.7 (acid) and 3.4 (calcined) nm by a more appropriate geometrical model informed by previous studies, see Supporting Information.[27]

To prepare NH_2-MSNs for fluorescence microscopy applications, we synthesized materials with TRITC dye covalently bound to the organically modified silica matrix (see Supporting Information for details). Inspection of these materials by TEM again reveals well-faceted nanoparticles and specific projections (Figure 1d). SAXS scattering patterns of acid-extracted samples in dry form (Figure 2c) were taken at CHESS. Twelve well-resolved peaks, consistent with the (200), (210), (211), (220), (310), (222), (320), (321), (400), (410), (420), and (421) indices of a cubic $Pm\bar{3}n$ lattice with unit cell dimension (a_0) = 9.9 nm can be observed for this fluorescent material (see below). Comparing Figure 1a and d with Figure 2a and c, the combined TEM and SAXS results suggest that TRITC molecules covalently bound to the silica matrix did not significantly alter the formation of a cubic $Pm\bar{3}n$ particle morphology. Average particle sizes as determined by TEM image analysis and DLS (about 215 ± 45 and 190 nm, respectively) showed slightly smaller particles as compared to non-dye modified NH_2-MSNs, while zeta potentials stayed highly positive (see Supporting Information Table S1).

It is known that pore sizes in mesoporous silica can be tailored by pore expander molecules.[28] To this end, we prepared large pore NH_2-MSNs with the aid of TMB (see Supporting Information). The TEM image in Figure 1e suggests that a quasi-periodic structure is preserved under these conditions, but that the resulting particles are smaller than those synthesized in the absence of TMB (compare panel e with panels b and c in Figure 1). Average particle sizes as observed from TEM image analysis and DLS are 110 ± 25 and 164 nm, respectively, that is, the TEM image analysis slightly underestimates sizes measured in solution. Repeated efforts to obtain SAXS diffractograms from acid-extracted large pore NH_2-MSNs only resulted in patterns (see Supporting Information S2a), in which the peaks are far less well resolved than those shown in Figure 2a−c, for the particles synthesized in the absence of TMB. Supporting Information Figure S2a also shows tic marks at the expected peak positions for a $Pm\bar{3}n$ lattice, assuming that the first order maximum is the (210) reflection. The broad second peak in the pattern would then correspond to where the (222), (320), and (321) peaks would appear. If one assumes $Pm\bar{3}n$ symmetry for the TMB acid-extracted material with strong peak at the (210) position, then the unit cell size for this material is 15.9 nm, that is, significantly larger than for materials synthesized without TMB, *vide supra*.

Zeta potential measurements on large pore NH_2-MSNs gave values comparable to those of materials synthesized in the absence of TMB (43 ± 7 mV). The N_2 sorption isotherms (Figure 3b) of acid-extracted and calcined large-pore aminated porous particles exhibit type IV isotherms with hysteresis loops. BET surface areas were determined as 780 $m^2\ g^{-1}$ for acid-extracted samples and 990 $m^2\ g^{-1}$ for calcined samples. The BJH (geometrical model) pore sizes were 5.3 (7.1) and 5 (6.6) nm for acid-extracted and calcined samples, respectively (Figure 3b, inset), that is, significantly larger than without TMB.

Elemental analysis confirmed amine contents as high as 20.45 and 23.38 mol % for aminated and large pore aminated MSNs, respectively (see Supporting Information). To the best of our knowledge, this is the highest amine content in ordered and porous silica nanoparticles reported to date.[29,30] Differences relative to previously reported synthesis protocols that may allow this high amine loading are the use of ethyl acetate and slightly lower pH (pH in our reaction is ~11, see Supporting Information).

Intensive research efforts have recently been devoted to the exploration of interactions between silica nanoparticles and cells.[3,20,21,26] To this end, herein, we report the study of endocytosis-mediated internalization of nanoparticles into COS-7 and epithelial cells (SLC-44) using PEGylated and TRITC-labeled NH_2-MSNs and large-pore NH_2-MSNs as imaging probes, respectively. For synthesis details, the interested reader is referred to the Supporting Information. TEM images of TRITC-labeled, large-pore NH_2-MSNs (Figure 1f) suggest that the combination of covalent incorporation of TRITC molecules into the aminated silica and use of the pore expander TMB did not significantly disturb the formation of a cubic particle structure. Interestingly, the average particle size as determined by TEM and DLS (see Supporting Information Table S1) went down to about 100 nm suggesting that the use of dye and pore expander together leads to the smallest sizes observed in this study. This is consistent with a particle size reduction for both of these synthesis variations separately (see Supporting Information Table S1). A SAXS pattern for this material is depicted in the Supporting Information (Figure S2b) and shows similar features as the diffractogram of large-pore NH_2-MSNs in Figure S2a.

Additional PEGylation with poly(ethylene glycol) succinimidyl succinate (PEG) prevented particle aggregation, providing good stability in physiological environments.[3,31] The change in zeta potentials before and after PEGylation from 36.5 ± 6 to −0.5 ± 5 mV for TRITC-labeled NH_2-MSNs and from 32 ± 6 to 6 ± 4 mV for TRITC-labeled large-pore NH_2-MSNs confirmed the surface modifications. At the same time through PEGylation, the hydrodynamic particle sizes as determined by DLS slightly increased for both samples (see Supporting Information Table S1). Confocal microscopy experiments confirm the uptake of normal and large-pore NH_2-MSNs into COS-7 and endothelial cells, respectively. Figure 4a,b illustrates the spontaneous cell uptake of PEGylated and TRITC-labeled NH_2-MSNs from the medium and accumulation into discrete cytosolic structures. Cell cross-section images along two orthogonal directions and obtained from z-scans in the

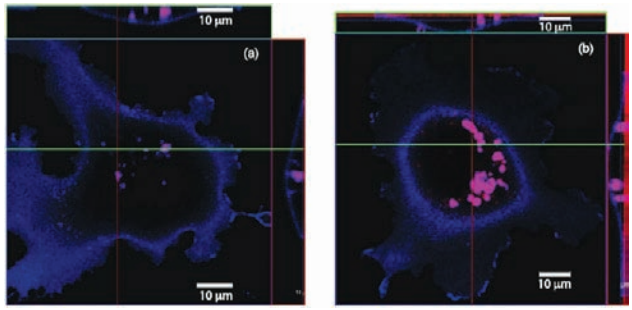

Figure 4. Confocal microscopy images of (a) endocytosed PEGylated and TRITC-labeled NH_2-MSNs into COS-7 cells and (b) endocytosed PEGylated and TRITC-labeled, large-pore NH_2-MSNs into epithelial cells. Particles appear in red. Far-red plasma membrane dye (Cell Mask Deep Red, Em/Ex 660/677 nm) was used to label the cell membrane (blue). Cell cross-section images along two orthogonal directions (red and green lines) are shown at the top and on the right of each image (see text) and corroborate the presence of particles inside the cells. Scale bars are 10 μm.

microscope shown at the top and on the right confirmed the presence of particles inside cells, most likely in endosomes. The size of particles used in the presented experiments is consistent with fluid phase endocytosis as the main particle uptake pathway. It is interesting to note that no particle aggregation was observed on the cell membrane consistent with successful PEGylation.

Acknowledgment. This work was supported by the Cornell Center for Materials Research (CCMR) with funding from a PREM program at Norfolk State University through the National Science Foundation (NSF) grant (DMR-0611430), by the Department of Energy grant DE-FG02-97ER62443 and by the National Institute of Dental and Craniofacial Research (R21DE018335). We thank the Cornell Universiy KAUST Center for Research and Education for financial support. This work was further supported by the U.S. Department of Homeland Security under Cooperative Agreement Number "2009-ST-108-LR0004". The authors thank CCMR for facility support. This work is based upon research conducted at the Cornell High Energy Synchrotron Source (CHESS), which is supported by the NSF and the National Institutes of Health/National Institute of General Medical Sciences under NSF award DMR-0225180. T.S. is grateful for a Thai Government Scholarship under the Ministry of Science and Technology.

Supporting Information Available: Detailed experimental methods, characterizations, and fluorescent imaging procedure. This material is available free of charge via the Internet at http://pubs.acs.org.

References

(1) De, M.; Ghosh, P. S.; Rotello, V. M. *Adv. Mater. (Weinheim, Ger.)* **2008**, *20*, 4225–4241.
(2) Park, K.; Lee, S.; Kang, E.; Kim, K.; Choi, K.; Kwon, I. C. *Adv. Funct. Mater.* **2009**, *19*, 1553–1566.
(3) Burns, A. A.; Vider, J.; Ow, H.; Herz, E.; Penate-Medina, O.; Baumgart, M.; Larson, S. M.; Wiesner, U.; Bradbury, M. *Nano Lett.* **2009**, *9*, 442–448.
(4) Tan, W. H.; Wang, K. M.; He, X. X.; Zhao, X. J.; Drake, T.; Wang, L.; Bagwe, R. P. *Med. Res. Rev.* **2004**, *24*, 621–638.
(5) Zhao, X. J.; Hilliard, L. R.; Mechery, S. J.; Wang, Y. P.; Bagwe, R. P.; Jin, S. G.; Tan, W. H. *Proc. Natl. Acad. Sci. U.S.A.* **2004**, *101*, 15027–15032.
(6) Burns, A.; Ow, H.; Wiesner, U. *Chem. Soc. Rev.* **2006**, *35*, 1028–1042.
(7) Piao, Y.; Burns, A.; Kim, J.; Wiesner, U.; Hyeon, T. *Adv. Funct. Mater.* **2008**, *18*, 3745–3758.
(8) Ow, H.; Larson, D. R.; Srivastava, M.; Baird, B. A.; Webb, W. W.; Wiesner, U. *Nano Lett.* **2005**, *5*, 113–117.
(9) Kim, S.; Ohulchanskyy, T. Y.; Pudavar, H. E.; Pandey, R. K.; Prasad, P. N. *J. Am. Chem. Soc.* **2007**, *129*, 2669–2675.
(10) Wan, Y.; Zhao, D. Y. *Chem. Rev.* **2007**, *107*, 2821–2860.
(11) Vallet-Regi, M.; Balas, F.; Arcos, D. *Angew. Chem., Int. Ed.* **2007**, *46*, 7548–7558.
(12) Fan, J.; Yu, C. Z.; Gao, T.; Lei, J.; Tian, B. Z.; Wang, L. M.; Luo, Q.; Tu, B.; Zhou, W. Z.; Zhao, D. Y. *Angew. Chem., Int. Ed.* **2003**, *42*, 3146–3150.
(13) Brohede, U.; Atluri, R.; Garcia-Bennett, A. E.; Stromme, M. *Curr. Drug Delivery* **2008**, *5*, 177–185.
(14) Li, J.; Wei, Y.; Deng, Y.; Gu, D.; Yang, X.; Zhang, L.; Tu, B.; Zhao, D. Y. *J. Mater. Chem.* **2010**, *20*, 6460–6463.
(15) Wang, J.; Zhou, H.; Sun, P.; Ding, D.; Chen, T. *Chem. Mater.* **2010**, *22*, 3829–3831.
(16) Che, S.; Sakamoto, Y.; Terasaki, O.; Tatsumi, T. *Chem. Lett.* **2002**, 214–215.
(17) Che, S.; Sakamoto, Y.; Terasaki, O.; Tatsumi, T. *Chem. Mater.* **2001**, *13*, 2237–2239.
(18) Kim, M. J.; Ryoo, R. *Chem. Mater.* **1999**, *11*, 487–491.
(19) Atluri, R.; Sakamoto, Y.; Garcia-Bennettt, A. E. *Langmuir* **2009**, *25*, 3189–3195.
(20) Vallhov, H.; Gabrielsson, S.; Stromme, M.; Scheynius, A.; Garcia-Bennett, A. E. *Nano Lett.* **2007**, *7*, 3576–3582.
(21) Lu, F.; Wu, S. H.; Hung, Y.; Mou, C. Y. *Small* **2009**, *5*, 1408–1413.
(22) Jin, H.; Heller, D. A.; Sharma, R.; Strano, M. S. *ACS Nano* **2009**, *3*, 149–158.
(23) Suteewong, T.; Sai, H.; Lee, J.; Bradbury, M.; Hyeon, T.; Gruner, S. M.; Wiesner, U. *J. Mater. Chem.* **2010**, *20*, 7807–7814.
(24) Huh, S.; Wiench, J. W.; Yoo, J. C.; Pruski, M.; Lin, V. S. Y. *Chem. Mater.* **2003**, *15*, 4247–4256.
(25) ^{29}Si NMR data supporting full incorporation will be discussed in detail in a forthcoming publication.
(26) Slowing, I.; Trewyn, B. G.; Lin, V. S. Y. *J. Am. Chem. Soc.* **2006**, *128*, 14792–14793.
(27) Ravikovitch, P. I.; Neimark, A. V. *Langmuir* **2002**, *18*, 1550–1560.
(28) Beck, J. S.; Vartuli, J. C.; Roth, W. J.; Leonowicz, M. E.; Kresge, C. T.; Schmitt, K. D.; Chu, C. T. W.; Olson, D. H.; Sheppard, E. W.; McCullen, S. B.; Higgins, J. B.; Schlenker, J. L. *J. Am. Chem. Soc.* **1992**, *114*, 10834–10843.
(29) Burleigh, M. C.; Markowitz, M. A.; Spector, M. S.; Gaber, B. P. *Chem. Mater.* **2001**, *13*, 4760–4766.
(30) Burleigh, M. C.; Markowitz, M. A.; Spector, M. S.; Gaber, B. P. *J. Phys. Chem. B* **2001**, *105*, 9935–9942.
(31) Kim, J.; Kim, H. S.; Lee, N.; Kim, T.; Kim, H.; Yu, T.; Song, I. C.; Moon, W. K.; Hyeon, T. *Angew. Chem., Int. Ed.* **2008**, *47*, 8438–8441.

JA1061664